SUPPLEMENTARY MATERIAL

HYBRID MULTIPLE-SITE MASS CLOSURE AND SOURCE APPORTIONMENT OF $PM_{2.5}$ AND AEROSOL ACIDITY AT MAJOR CITIES IN THE PO VALLEY

Mauro Masiol[a,b,c*], Stefania Squizzato[a,b,c], Gianni Formenton[d], Md. Badiuzzaman Khan[c,e], Philip K. Hopke[b,f], Athanasios Nenes[a,g], Spyros N. Pandis[a,h,i], Laura Tositti[j], Francesca Benetello[c], Flavia Visin[c], Bruno Pavoni[c]

[a] Institute of Chemical Engineering Sciences, Foundation for Research and Technology - Hellas (FORTH), GR-26504 Patras, Greece
[b] Department of Public Health Sciences, University of Rochester Medical Center, Rochester, NY 14642, United States
[c] Dipartimento di Scienze Ambientali, Informatica e Statistica, Università Ca' Foscari Venezia, IT-30170 Mestre-Venezia, Italy
[d] Dipartimento Regionale Laboratori, Agenzia Regionale per la Prevenzione e Protezione Ambientale del Veneto (ARPAV), IT- 30174 Mestre-Venezia, Italy
[e] Department of Environmental Science, Bangladesh Agricultural University, Mymensingh 2202, Bangladesh
[f] Center for Air Resources Engineering and Science, Clarkson University, Potsdam, NY 13699-5708, United States
[g] Laboratory of Atmospheric Processes and their Impacts, School of Architecture, Civil and Environmental Engineering, École Polytechnique Fédérale de Lausanne, Lausanne, CH-1015, Switzerland
[h] Department of Chemical Engineering, University of Patras, Patras, Greece
[i] Department of Chemical Engineering, Carnegie Mellon University, Pittsburgh, PA 15213, USA
[j] Dipartimento di Chimica "G. Ciamician", Alma Mater Studiorum Università di Bologna, IT-40126 Bologna, Italy

[*] To whom correspondence should be addressed.
(Mauro Masiol) Email: mauro.masiol@gmail.com

Section S1. Site characteristics.

A multiple-site $PM_{2.5}$ sampling campaign was carried out from April 2012 to March 2013 in 6 major cities of the Veneto region: Belluno (BL), Conegliano (TV), Vicenza (VI), Venice-Mestre (VE), Padua (PD) and Rovigo (RO) (Figure S1a). Stations are managed by the Environmental Protection Agency for the Veneto Region (ARPAV, Agenzia Regionale per la Prevenzione e Protezione Ambientale del Veneto, http://www.arpa.veneto.it/). Sites are placed in high density residential areas and can be considered as representative of city-wide background $PM_{2.5}$ concentrations.

Up today, the literature offers only three air quality studies extended to the whole Veneto region:

(1) a trend analysis of major air pollutants (nitrogen oxides, ozone, sulfur dioxide, carbon monoxide and bulk PM_{10} and $PM_{2.5}$) during 2008-2014 and measured at 43 sites (including all the sites used in this study) (Masiol et al., 2017);

(2) the analysis of PM10-bound PAHs over 21 sites (including BL, VE, PD and RO) (Masiol et al., 2013);

(3) the analysis of a large folk fire event occurring on 5^{th}-6^{th} January and measured at 32 sites (including all the sites used in this study) (Masiol et al. 2014a),

On the contrary, mass closure and source apportionment studies were only performed at the Veneto capital city, Venice-Mestre for $PM_{2.5}$ (Masiol et al., 2014b; Squizzato et al., 2014) or PM_1 (Squizzato et al., 2016), but never using VE as a sampling site. Instead, VE site was previously used for other studies on PM_{10} elemental composition (Rampazzo et al., 2008) or long-term trends (2000-2013) of air pollutants (Masiol et al., 2014c). Another source apportionment study (Squizzato et al., 2017), limited to wintertime, was performed in Treviso (a city roughly between the VE and TV sites of this study).

Site characteristics are listed in Table S1. Figure S2 reports the results of a buffer analysis (circular buffers of 5 km radii centered on each site) performed on the 2012 land cover data (EEA CORINE CLC2012; EEA, 2019). Demographic data refer to Italian National Census 2011 and to the whole municipalities (ISTAT, 2019). Table S2 summarizes the emissions at Municipality level for 2013.

- **BL** (36,600 inhabitants) is located in an Alpine valley (height ~390 m) surrounded by mountains (height ranging from ~700 to ~2500 m), with no large industries or heavy traffic. Biomass burning emissions are intense in winter, as wood is largely used for domestic heating.
- **TV** (35,700 inhabitants) is located in a foothill region and is therefore representative of the transition between the mountain and lowland. Industrial plants include factories to process stainless steel, appliances and electrical equipment. A large part of the land use is dedicated to agriculture, especially for vineyards (Prosecco wine).
- **VI** (115,900 inhabitants) is a large city with intense traffic and small to medium-sized mechanical, textile, tanning, jewelry manufactures, and steelworks (steel recycling).
- **VE** (271,000 inhabitants) represents a large conurbation extending from the coastal lagoon of Venice to the mainland. It is often referred as the "metropolitan area of Venice", encompassing several municipalities. The emissive scenario includes heavy road, maritime and airport traffic, an industrial zone hosting chemical and steel plants, an oil-refinery, incineration facilities, thermoelectric power plants (coal+waste), large shipping yards, and other factories.
- **PD** (214,200 inhabitants) is the most densely populated municipality of the region, with many medium-sized factories mainly in the engineering, technological and building sectors, but it also suffers from intense traffic due to the presence of a large intermodal and logistics hub. A large waste incinerator is also present in the city.
- **RO** (52,800 inhabitants) is located in a flat lowland midway between the Alps and the Apennines and is the biggest processing center of Veneto for agricultural products.

Section S2. CWT details.

Single-site CWT. Essentially, the geographic region around the receptor site is divided into an array of equally-spaced grid cells of longitude *i* and latitude *j*, with a domain defined by the extension of all trajectories. Then, a weighted concentration $CWT_{i,j}$ is assigned to each *i*,*j*-th cell as:

$$CWT_{i,j} = \frac{\sum_{t=1}^{T} C_t \tau_{i,j,t}}{\sum_{t=1}^{T} \tau_{i,j,t}} \cdot W_{i,j}$$

where *T* is the total number of back-trajectories, *t* [1, T] is the index of each trajectory, C_t is the concentration measured at one receptor site on the arrival (starting time) of the back-trajectory *t*, and $\tau_{i,j,t}$ is the endpoint number for the trajectory *t* in the *i*,*j*–th cell, i.e. it represents time spent in the grid cell by that trajectory. $W_{i,j}$ represents weighting functions applied to the results. In facts, CWT may be affected by the "*trailing effect*," i.e., grid points covered by high numbers of endpoints return statistically stable CWT values, while the values for cells covered by few endpoints may be misestimated. Weighting functions $W1_{i,j}$ and $W2_{i,j}$ were therefore used to downgrade CWT values of PMF source contributions or pH and ΔpH.

Weighting functions for PMF source contributions. A weighting function $W1_{i,j}$ was used to downgrade CWT values in cells where the number of endpoints $N_{i,j}$ is within the 4 quartiles of the distribution of all $N_{i,j}$ over the domain:

$$W1_{i,j} = \begin{cases} CWT \cdot 1 & N_{i,j} \geq 75\text{th percentile} \\ CWT \cdot 0.75 & 50\text{th} \leq N_{i,j} < 75\text{ th percentile} \\ CWT \cdot 015 & 25\text{th} \leq N_{i,j} < 50\text{ th percentile} \\ CWT \cdot 0.05 & N_{i,j} < 25\text{th percentile} \end{cases}$$

The multiplicative values used in W1 were selected after many tests and according to previous published literature (Masiol et al., 2019). Maps showing $N_{i,j}$ for the sites are reported in Figure S15.

Weighting functions for pH and ΔpH. A simpler weighting function $W2_{i,j}$ was used to remove endpoints with $N_{i,j}$<75th percentile for pH and ΔpH:

$$W2_{i,j} = \begin{cases} CWT & N_{i,j} \geq 75\text{th percentile} \\ N/A & N_{i,j} < 75\text{th percentile} \end{cases}$$

Final combined (multiple-site) CWT (MS-CWT). CWT were separately calculated for 5 sites (all sites except BL). The single CWT calculated at all the sites were averaged to obtain a mean value, $\overline{CWT_{i,j}}$, i.e.:

$$\overline{CWT_{i,j}} = \left[\sum_{n=1}^{N} \left(\frac{\sum_{t=1}^{T} C_{t,n} \tau_{i,j,t,n}}{\sum_{t=1}^{T} \tau_{i,j,t,n}} \cdot W_{i,j,n} \right) / N \right]$$

Due to the relative closeness of the 5 sites in the lower end of the Po Valley (max distance TV-RO ~100 km), the domain covered by single CWTs is very similar at all the sites (Figure S15). However, a few endpoints on the edges of single CWT domains may not present CWT values

calculated at all the sites. Therefore, weighting functions $Z1_{i,j}$ and $Z2_{i,j}$ were used to downgrade $\overline{\mathrm{CWT}}$ in cells with values not calculated at all the single sites for PMF source contributions ($Z1_{i,j}$) and pH-ΔpH ($Z2_{i,j}$), respectively:

$$Z1_{i,j} = \begin{cases} \overline{CWT} \cdot 1 & 5 \text{ sites} \\ \overline{CWT} \cdot 0.75 & 4 \text{ sites} \\ \overline{CWT} \cdot 0.5 & 3 \text{ sites} \\ \overline{CWT} \cdot 0 & < 3 \text{ sites} \end{cases}$$

$$Z2_{i,j} = \begin{cases} \overline{CWT} & \geq 3 \text{ sites} \\ N/A & < 3 \text{ sites} \end{cases}$$

These weighting functions were arbitrarily chosen and aim to increase the robustness of the MS-CWT by removing endpoints where less than 3 single CWT have been calculated. In addition, the function $Z1_{i,}$ (applied to the PMF factors) also downgrades the $\overline{\mathrm{CWT}}$ in cells with values calculated only in 3 or 4 sites.

A further smoothing of the MS-CWT was also performed using an isotropic Gaussian kernel with standard deviation 0.75 for obtaining a better rendering and to partially account for the noise and uncertainty associated with trajectory models.

Table S1. Site characteristics and analyzed air pollutants (other than $PM_{2.5}$ samples collected for this study). Coordinates: WGS84.

Site	Municipality – Site full name	Lat. (N)	Long. (E)	Altitude (m a.s.l.)	Site characteristic	Analyzed air pollutants
BL	Belluno – BL città	46.143	12.218	401	Public park in residential/commercial area	CO, NO_x, O_3, SO_2, PM_{10}
TV	Conegliano - Conegliano	45.89	12.307	72	Residential area	CO, NO_x, O_3, SO_2, PM_{10}
VI	Vicenza – Quartiere Italia	45.56	11.539	36	Residential area	CO, NO_x, O_3, PM_{10}
VE	Venice – Mestre Parco Bissuola	45.498	12.261	1	Public park, residential area	CO, NO_x, O_3, SO_2, PM_{10}
PD	Padova - Mandria	45.371	11.841	13	Residential area	CO, NO_x, O_3, SO_2, PM_{10}
RO	Rovigo – RO Centro	45.074	11.782	7	Residential-commercial area	CO, NO_x, O_3, SO_2, PM_{10}

Table S2. Emission inventories for 2013 (INEMAR; ARPAV, 2019) at Municipality level. VOCs= volatile organic compounds. SNAP macro-sectors: SNAP1= combustion in energy and transformation industries; SNAP3= combustion in manufacturing industry; SNAP4= production processes; SNAP7= road transport; SNAP8= other mobile sources and machinery; SNAP9= waste treatment and disposal.

	$PM_{2.5}$	Ni	As	Cd	Pb	BaP	SO_2	NO_x	NH_3	VOCs
	ton/y	*kg/y*	*kg/y*	*kg/y*	*kg/y*	*kg/y*	*ton/y*	*ton/y*	*ton/y*	*ton/y*
All macro-sectors										
Belluno	110.0	1.1	0.3	3.1	11.4	37.0	11.5	252.1	93.6	766.1
Conegliano	62.9	1.0	0.4	1.8	10.3	18.2	4.5	275.7	37.7	496.2
Vicenza	118.5	19.1	94.1	9.8	293.7	21.8	210.0	1334.0	155.2	1483.9
Venezia	405.1	530.8	49.6	9.4	115.3	27.1	3358.0	9862.5	194.8	3043.6
Padova	180.5	78.0	99.8	21.6	266.2	26.6	95.6	1930.5	227.7	2397.7
Rovigo	59.6	11.9	1.4	2.7	19.8	12.4	11.7	480.4	199.5	1147.8
Industrial sectors (SNAP1+3+4+9)										
Belluno	0.2	0.0	0.0	0.0	0.0	0.0	0.0	5.9	0.0	10.6
Conegliano	0.3	0.0	0.0	0.0	0.0	0.0	0.1	9.6	0.0	31.4
Vicenza	6.4	16.2	92.9	6.7	268.3	0.9	202.1	286.2	0.0	111.5
Venezia	47.6	327.1	42.2	3.8	59.6	0.1	2977.9	4872.0	13.4	166.0
Padova	33.2	72.9	97.5	16.8	219.0	0.6	82.9	352.0	1.0	152.4
Rovigo	1.4	10.4	0.8	1.0	6.4	0.2	9.2	19.2	4.5	18.4
Transports (SNAP7+8)										
Belluno	14.7	0.4	0.1	0.1	3.6	0.2	1.2	179.8	1.3	69.8
Conegliano	11.3	0.5	0.2	0.2	5.4	0.3	0.3	217.4	3.4	73.8
Vicenza	48.7	1.6	0.8	0.6	15.2	1.0	2.0	907.7	12.7	243.7
Venezia	266.8	201.1	6.2	1.6	35.7	2.0	364.5	4639.0	20.7	1029.5
Padova	62.3	2.9	1.3	1.2	29.1	1.6	1.7	1279.2	21.6	428.2
Rovigo	20.3	0.9	0.4	0.3	8.2	0.5	0.5	397.9	7.1	115.8

Table S3. Conversion factors and equations used in the mass closure.

MC component	Acronym	Conversion factors	References	Note
Organic matter	**OM**	1.6·OC	Marcazzan et al. (2001); Perrone et al. (2012); Squizzato et al. (2016)	–
Elemental carbon	**EC**	EC	–	–
Crustal material (aka dust or geological material)	**CRU**	(1.89·Al)+(2.14·Si)+(1.4·Ins.Ca)+(1.2·Ins.K)+(1.43·Fe)+(1.67·Ti)	Andrews et al (2000), but only accounting for insoluble K and Ca, instead of total K and Ca	Si (not analyzed) is derived from the Si/Al ratio (2.17) in PM_{10} sampled in Veneto (Masiol et al., 2012). Insoluble Ca and K are calculated as total Ca-Ca^{2+} and total K-K^{+}, respectively
Secondary inorganic aerosol	**SIA**	SO_4^{2-}+NO_3^{-}+NH_4^{+}	E.g., Chow et al. (1994); Maenhaut et al. (2002)	–
Other ions	**OI**	Cl^{-}+Na^{+}+Mg^{2+}+K^{+}+Ca^{2+}	–	Sum of major inorganic ions not used for SIA
Trace elements	**TRACE**	V+Mn+Co+Ni+Cu+Zn+As+Cd+Sb+Ba+Pb	–	Sum of all analyzed elements not used for CRU

Table S4. Chemical species as inputted to the final PMF model.

Species	Category	% Modeled Samples
$PM_{2.5}$	Weak	99
OC	Strong	99
EC	Strong	98
F^-	Bad	0
Cl^-	Weak	99
NO_3^-	Strong	99
SO_4^{2-}	Strong	99
Na^+	Weak	94
NH_4^+	Strong	99
K^+	Strong	99
Mg^{2+}	Bad	0
Ca^{2+}	Bad	0
Mg	Weak	97
Al	Strong	99
S	Bad	0
K	Bad	0
Ins. K	Bad	0
Ca	Strong	96
Ins. Ca	Bad	0
Ti	Strong	99
V	Strong	99
Mn	Strong	98
Fe	Strong	98
Co	Bad	0
Ni	Strong	98
Cu	Strong	98
Zn	Strong	96
As	Bad	0
Cd	Bad	0
Sb	Strong	99
Ba	Weak	98
Pb	Strong	99
BaA	Weak	99
Chry	Weak	99
BbF	Weak	99
BkF	Weak	99
BaP	Weak	99
DBahA	Weak	99
IP	Weak	99
BghiP	Weak	99
Total PAH	Bad	0

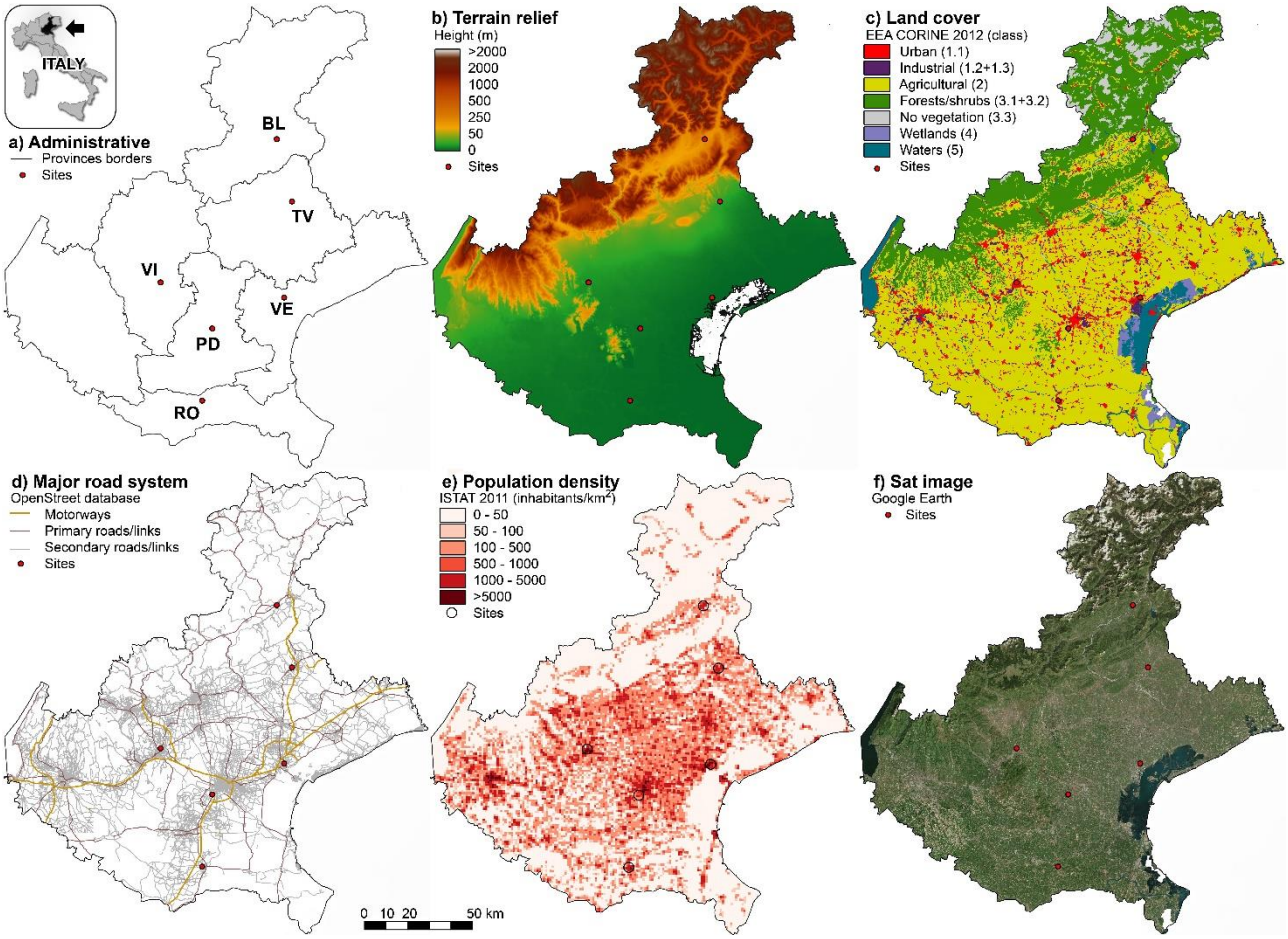

Figure S1. Maps of the Veneto region and sampling sites. From top-left to bottom-right: (a) administrative borders (ISTAT, 2019); (b) terrain relief from digital elevation model; (c) land-cover from EEA CORINE land-cover database (EEA, 2019); (d) major road systems from OpenStreet.org; (e) population density from 2011 census (ISTAT, 2019); (f) satellite image from GoogleEarth.

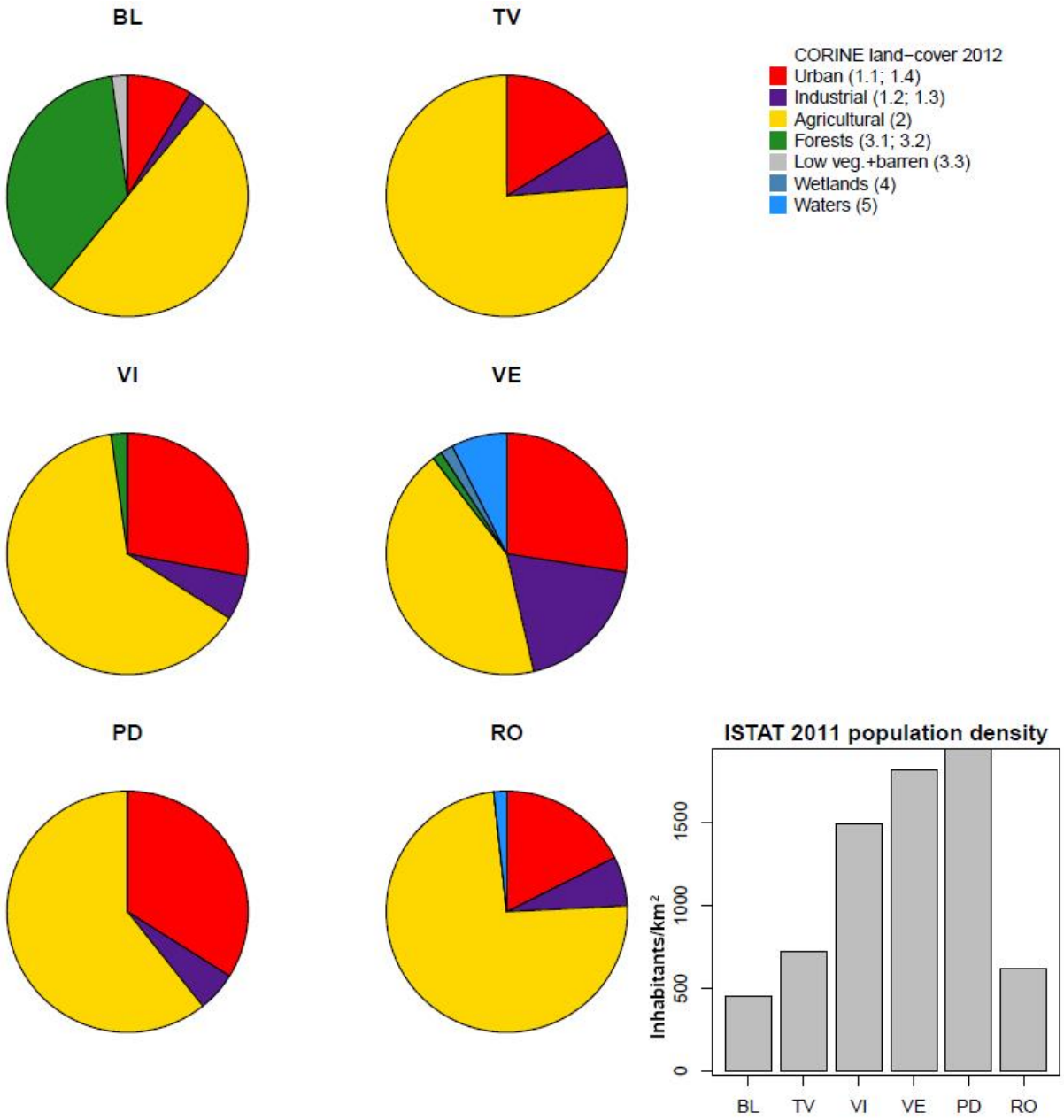

Figure S2. Pie charts reporting the percent land cover (PLC) in a buffer circle of 5 km radius from each sampling site. Land cover data are taken from the EEA CORINE land-cover database (EEA, 2019). The bar-chart (bottom-right) represents the average population density within buffer circles of 5 km radius for each sampling site. Data are taken from the National Census 2011 (ISTAT, 2019).

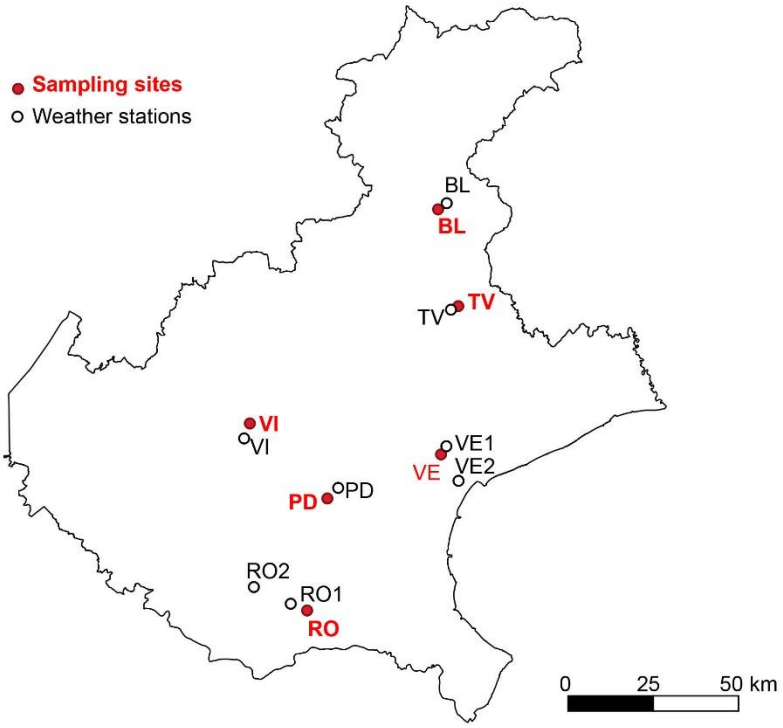

Figure S3. Location of the weather stations and $PM_{2.5}$ sites used in this study.

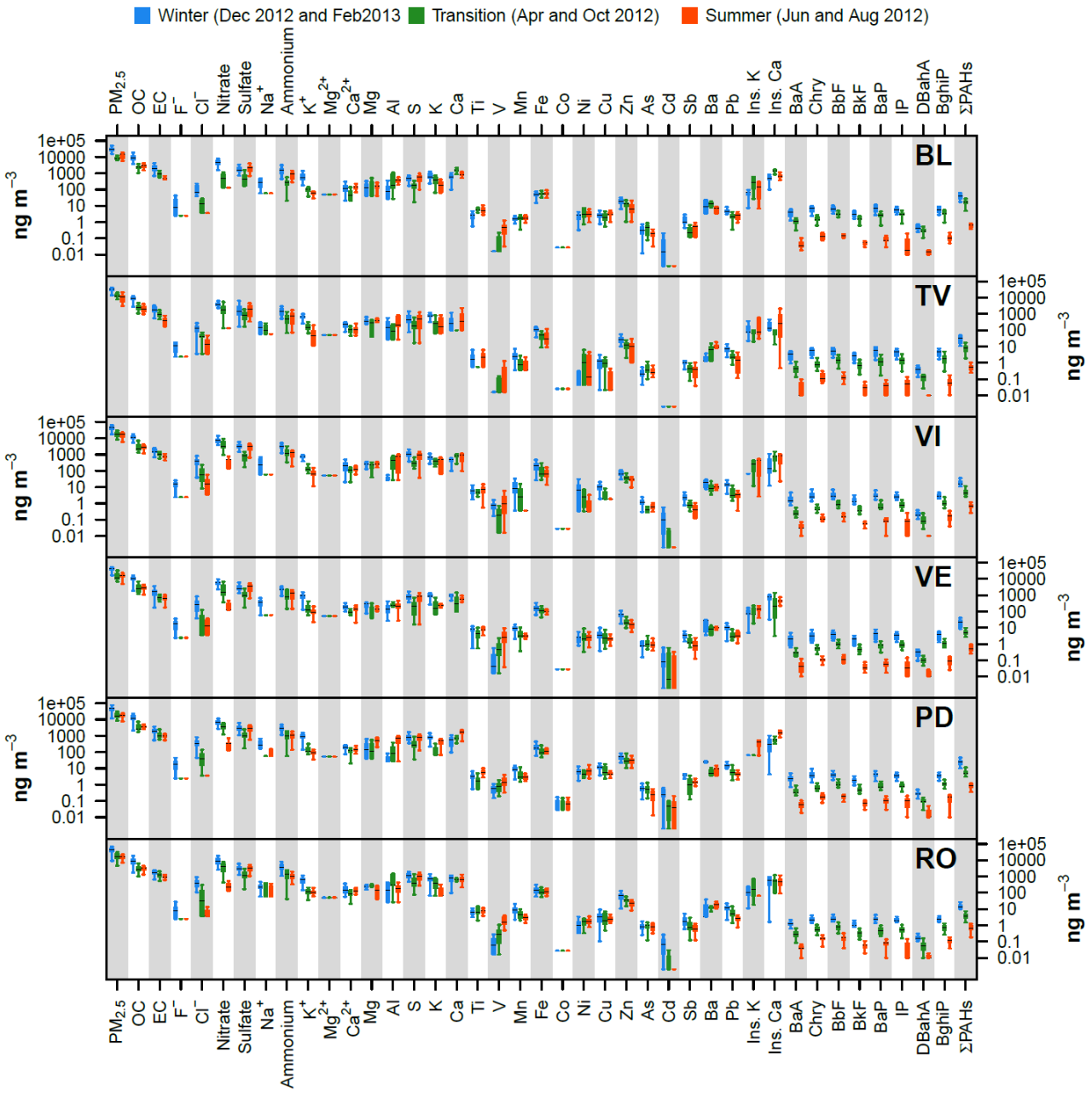

Figure S4. Boxplots of the analyzed compounds and elements in $PM_{2.5}$ at the six sampling sites in each season. For each species and site, the boxplots are clustered to show the distributions in the three seasons (boxplots: line=median, box=inter-quartile range, whiskers=±1.5*inter-quartile range; outliers and extremes are not shown).

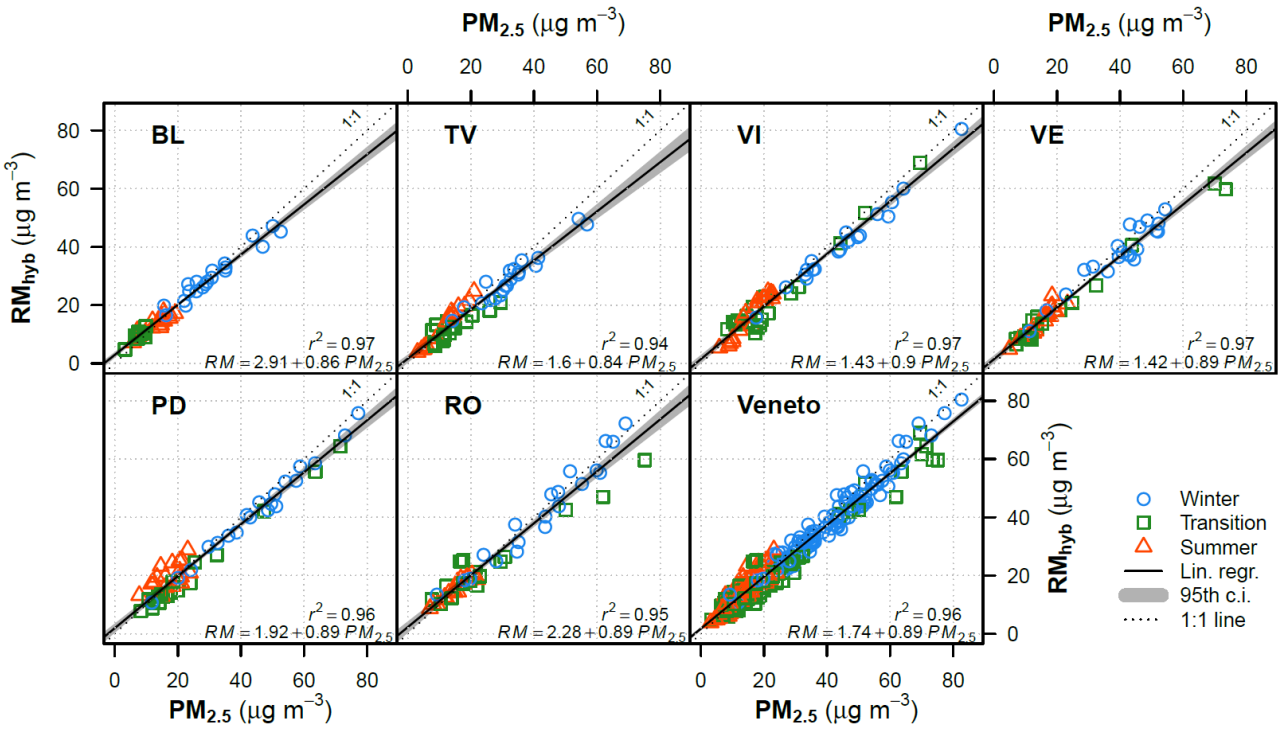

Figure S5a. Results of the hyb-MS- MC with the ISORROPIA-II solutions for the "base" simulations showing the multiple linear regressions between the reconstructed $PM_{2.5}$ mass concentrations (dependent variable) and measured $PM_{2.5}$ mass concentrations (independent variable) at each site and combined (Veneto: all sites). The 95% confidence intervals (c.i.) of linear regressions are also reported.

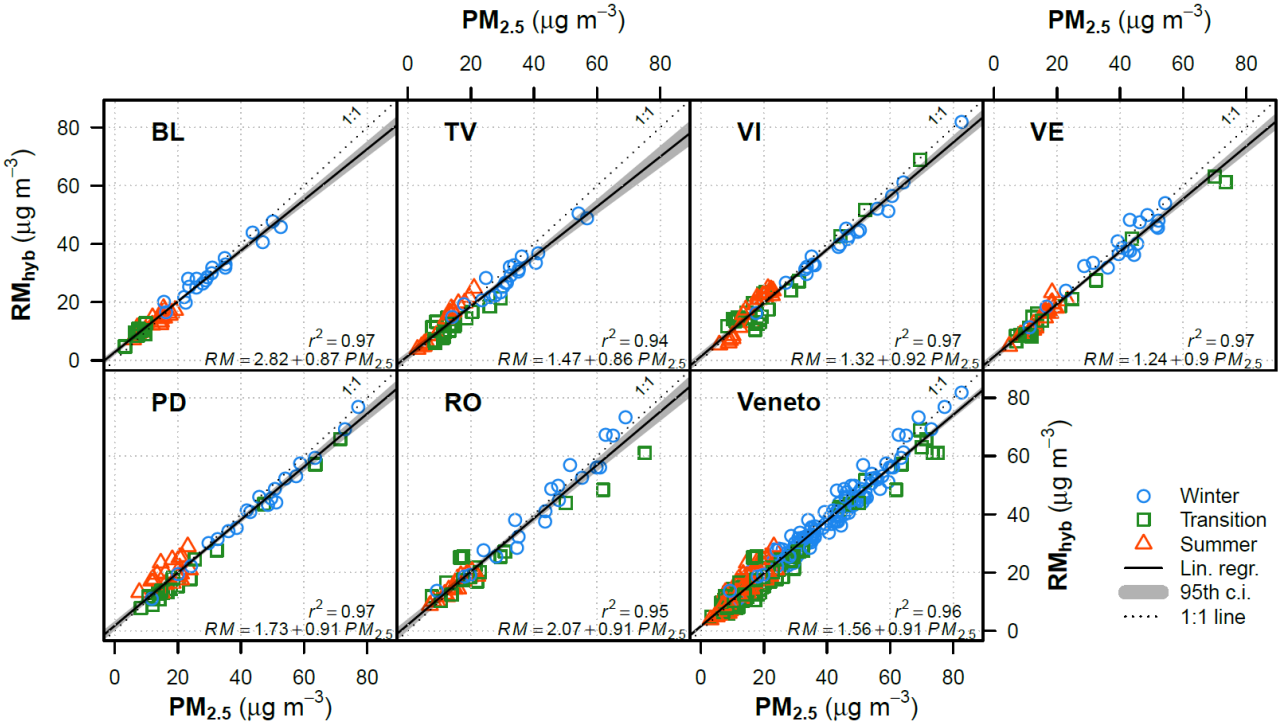

Figure S5b. Results of the hyb-MS- MC with the ISORROPIA-II solutions for the "average" results showing the multiple linear regressions between the reconstructed $PM_{2.5}$ mass concentrations (dependent variable) and measured $PM_{2.5}$ mass concentrations (independent variable) at each site and combined (Veneto: all sites). The 95% confidence intervals (c.i.) of linear regressions are also reported.

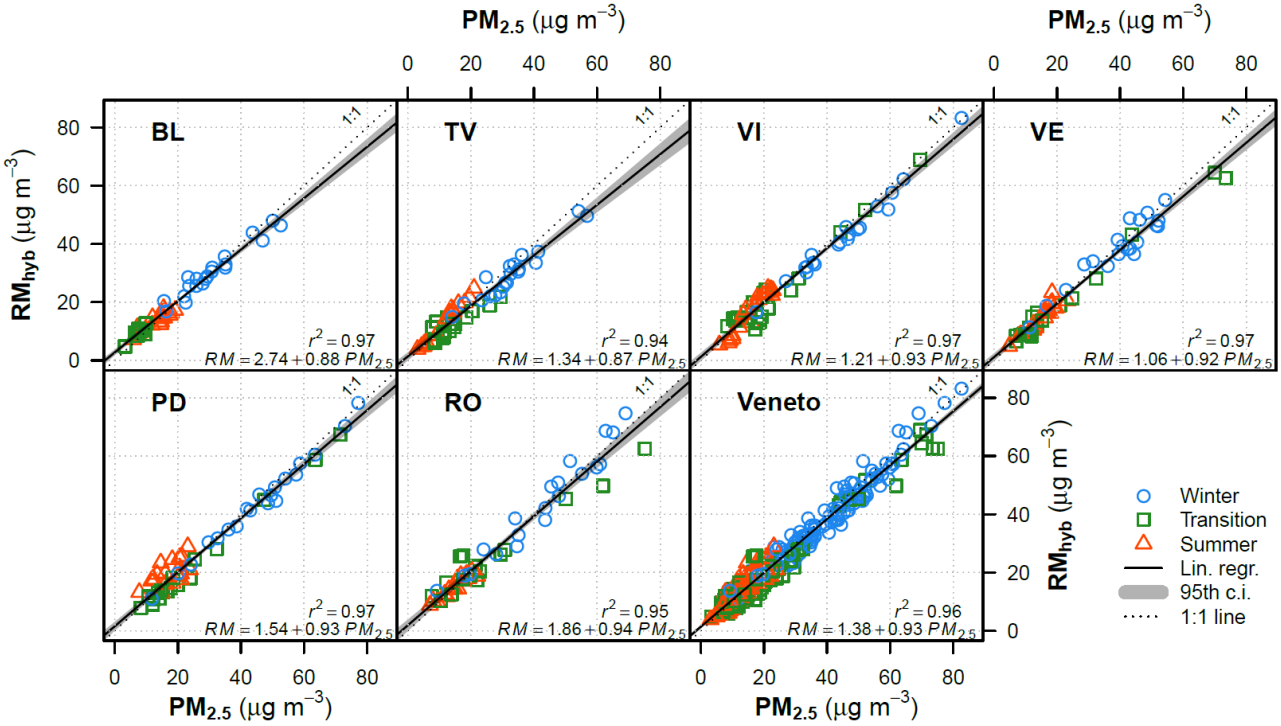

Figure S5c. Results of the hyb-MS- MC with the ISORROPIA-II solutions for the "sensitivity" tests showing the multiple linear regressions between the reconstructed $PM_{2.5}$ mass concentrations (dependent variable) and measured $PM_{2.5}$ mass concentrations (independent variable) at each site and combined (Veneto: all sites). The 95% confidence intervals (c.i.) of linear regressions are also reported.

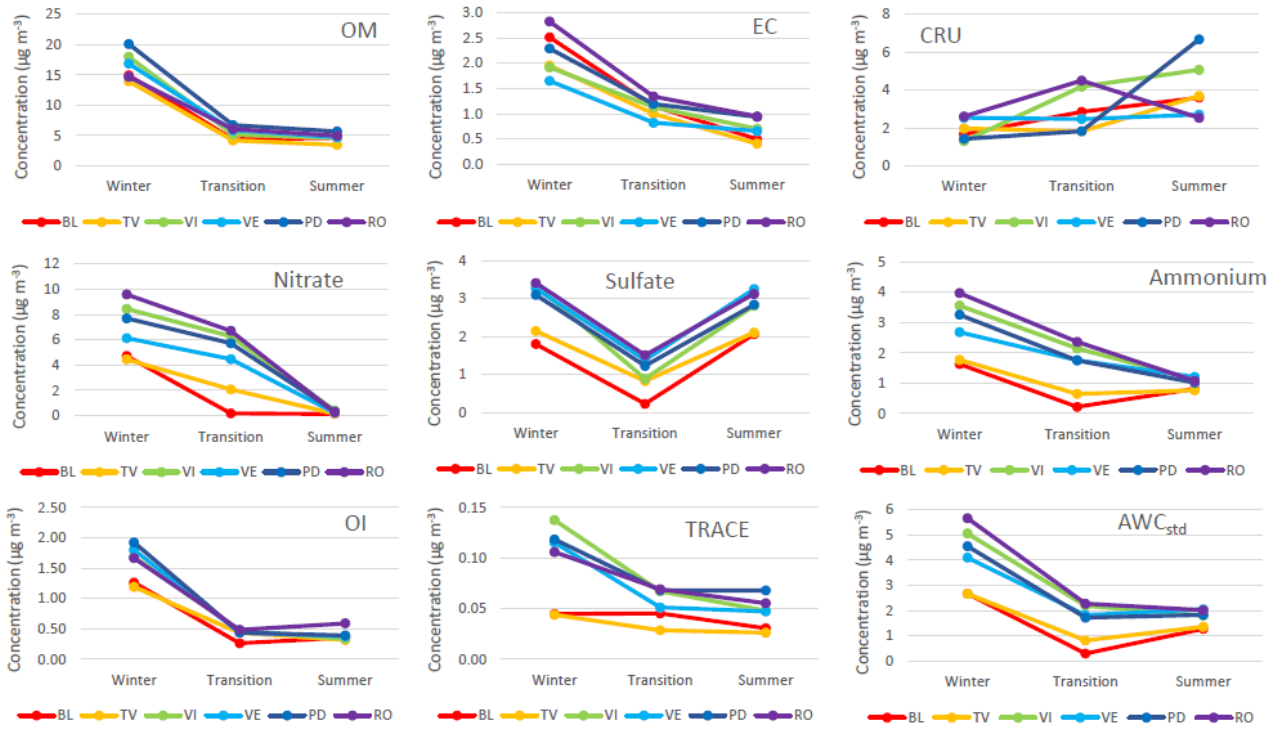

Figure S6. Seasonal averaged concentrations of major chemical components derived from the hyb-MS-MC with the "average" ISORROPIA-II model.

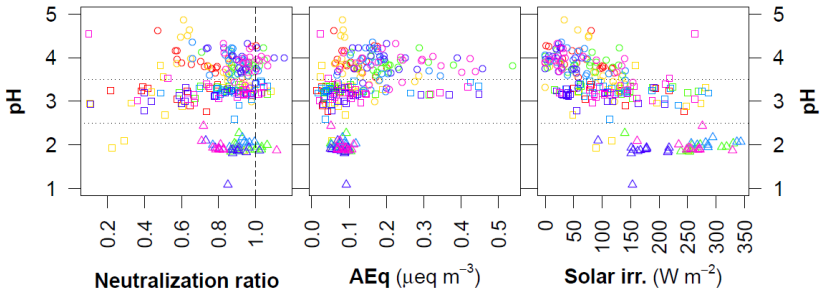

Figure S7. Scatterplots showing the relationship between pH (modelled by ISORROPIA-II, "average") and neutralization ratio, AEq and measured solar irradiation. Other relationships are provided in Figure 3. The neutralization ratio (Bencs et al., 2008; Engelhart et al., 2011), a proxy to estimate the degree of neutralization of sulfate and nitrate by ammonium (expressed as equivalent), was calculated as: $NR = [NH_4^+]/([SO_4^{2-}] + [NO_3^-])$.

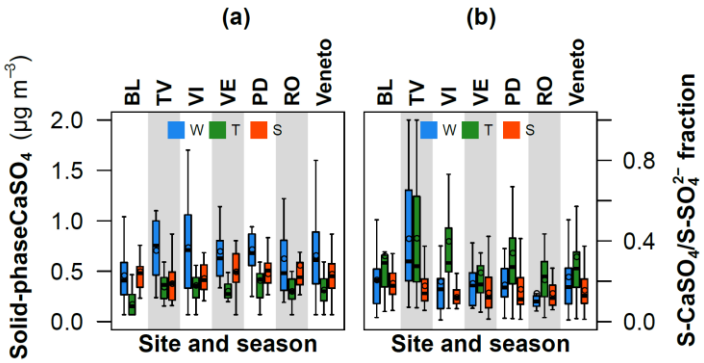

Figure S8. (a) Solid-phase $CaSO_4$ and (b) S-$CaSO_4$ to S-SO_4^{2-} ratios derived from ISORROPIA-II. Data refer to the "average" results. The boxplots show the distribution of estimated values at all the single sites and combined (6 cities= Veneto); W=winter, T= transition, S= summer.

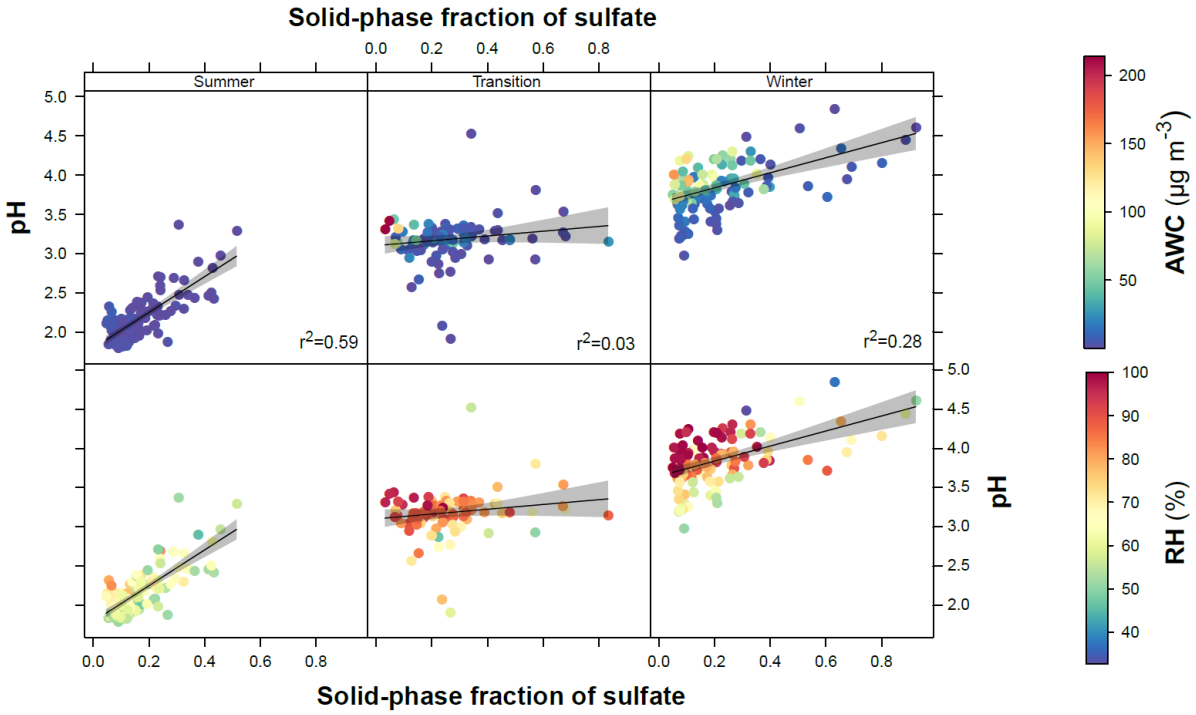

Figure S9. Scatterplots of the solid-phase fraction of sulfate (as solid $CaSO_4$) against pH modeled by ISORROPIA-II by season and their regression lines. The color of points shows the AWC (upper) and RH (bottom). Regression lines (black line) and their 95th confidence intervals (grey) are shown.

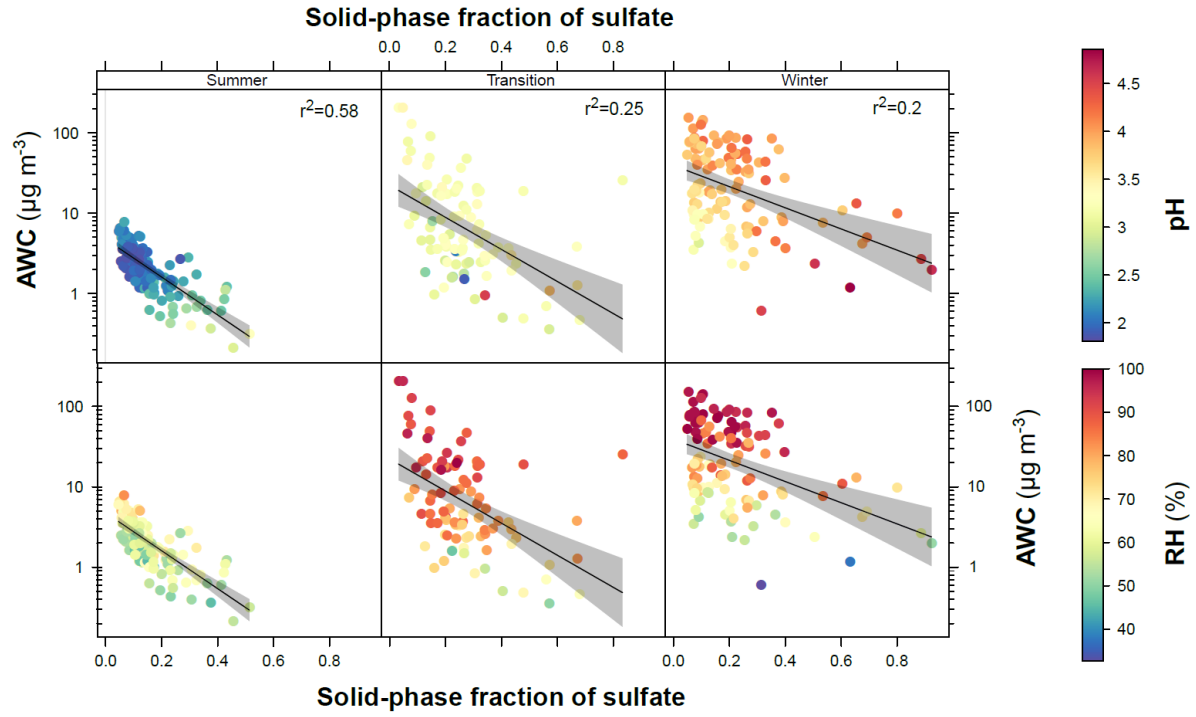

Figure S10. Scatterplots of the solid-phase fraction of sulfate (as solid $CaSO_4$) against AWC modeled by ISORROPIA-II by season and their regression lines. The color of points shows the pH (upper) and RH (bottom). Regression lines (black line) and their 95th confidence intervals (grey) are shown.

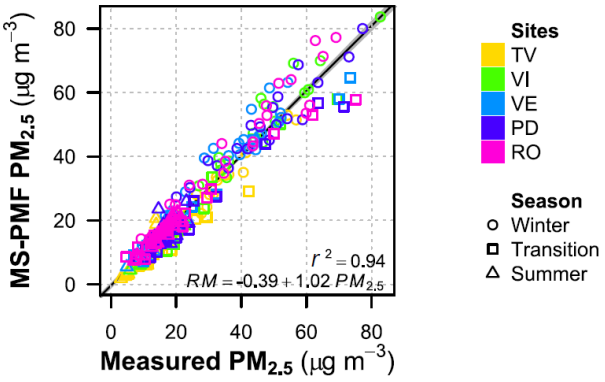

Figure S11. Results of the MS-PMF. Regression between measured and modeled $PM_{2.5}$ concentrations (left) and combined (5 sites) cumulative source contributions over all the study period.

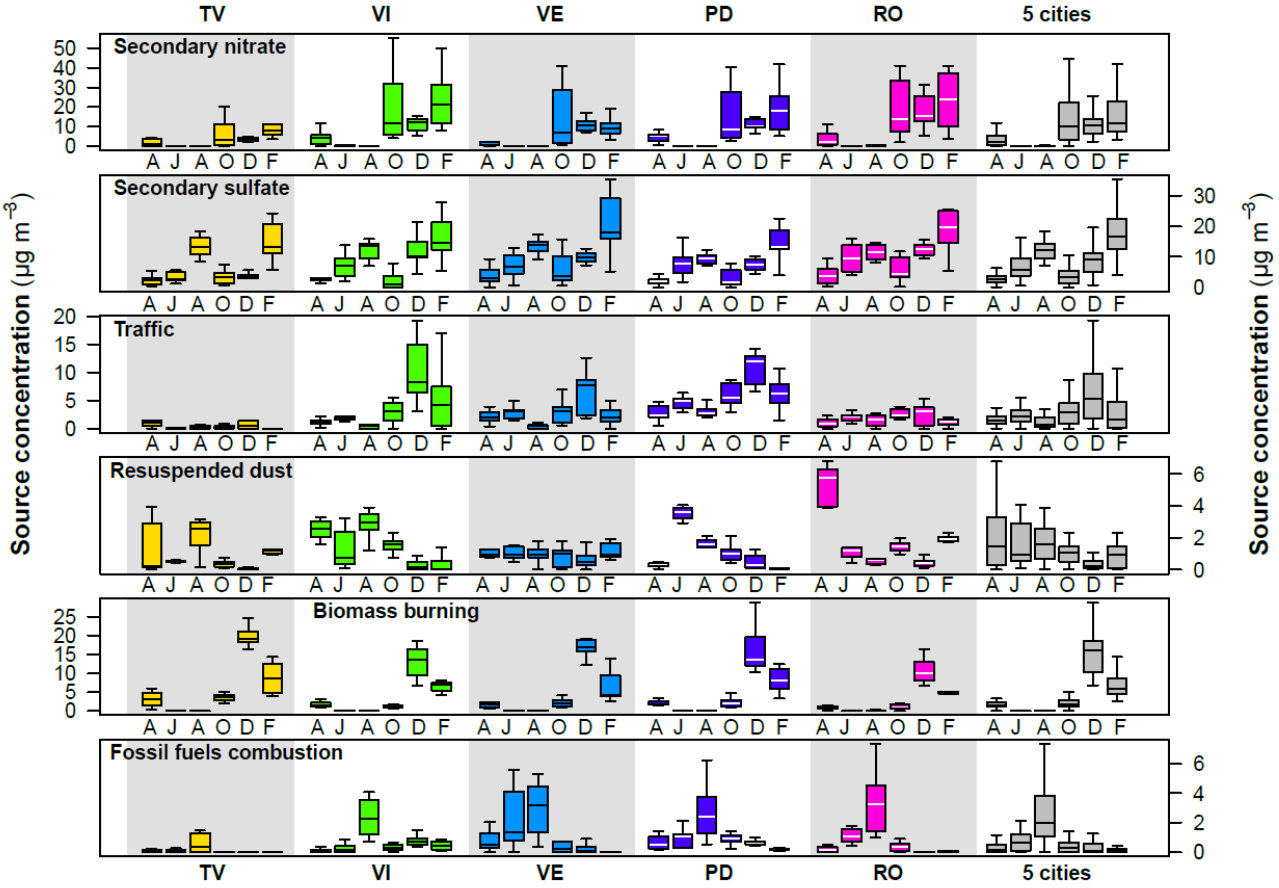

Figure S12. Boxplots of MS-PMF source contributions categorized by month and site/combined (5 sites). A J A O D F= April – June – August – October – December – February.

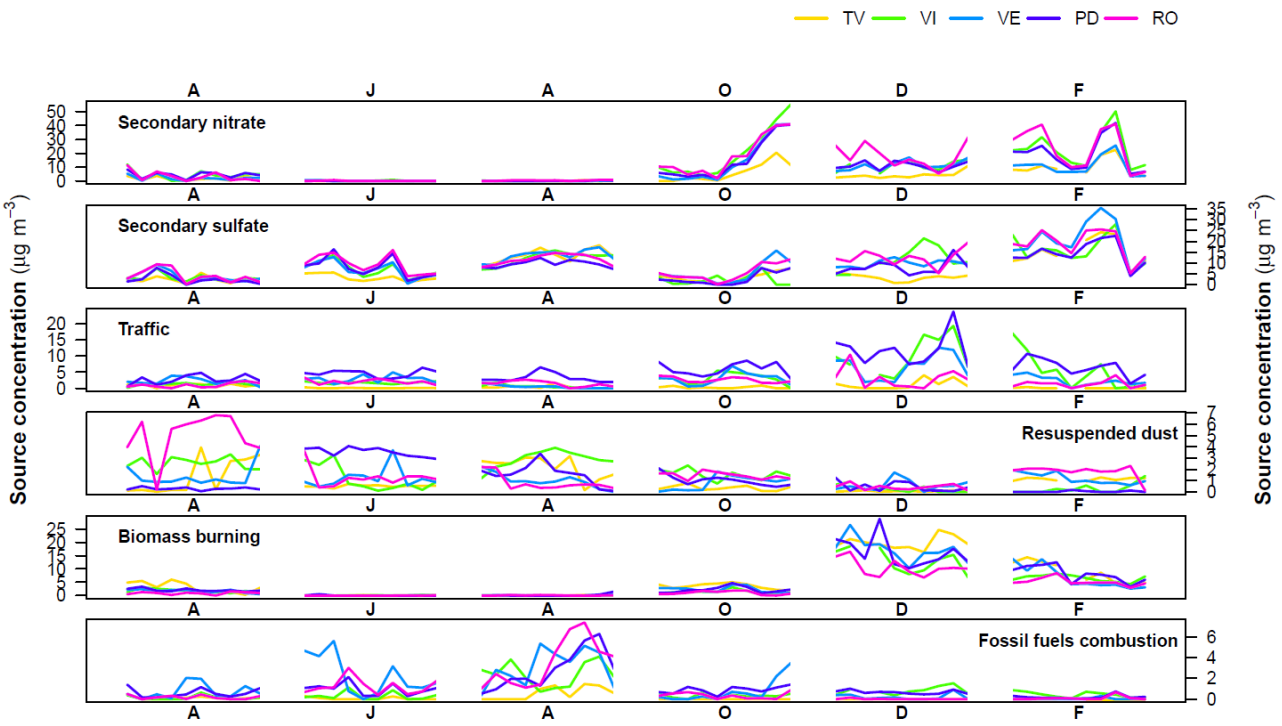

Figure S13. Time series of the MS-PMF source contributions categorized by month and site/combined (5 sites).

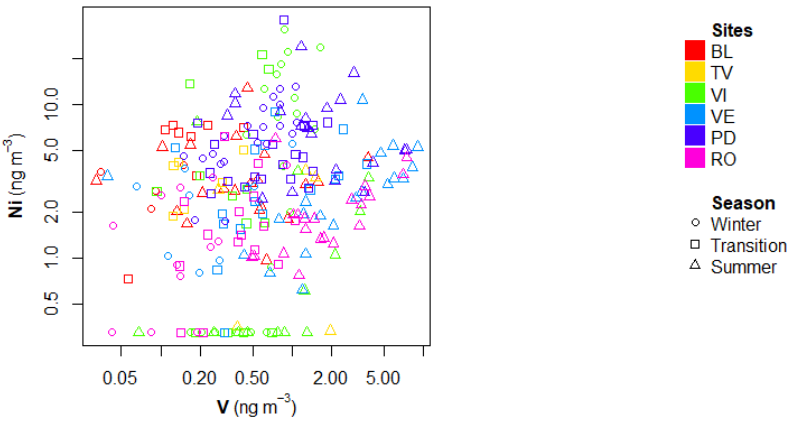

Figure S14. Scatterplot of V and Ni concentrations.

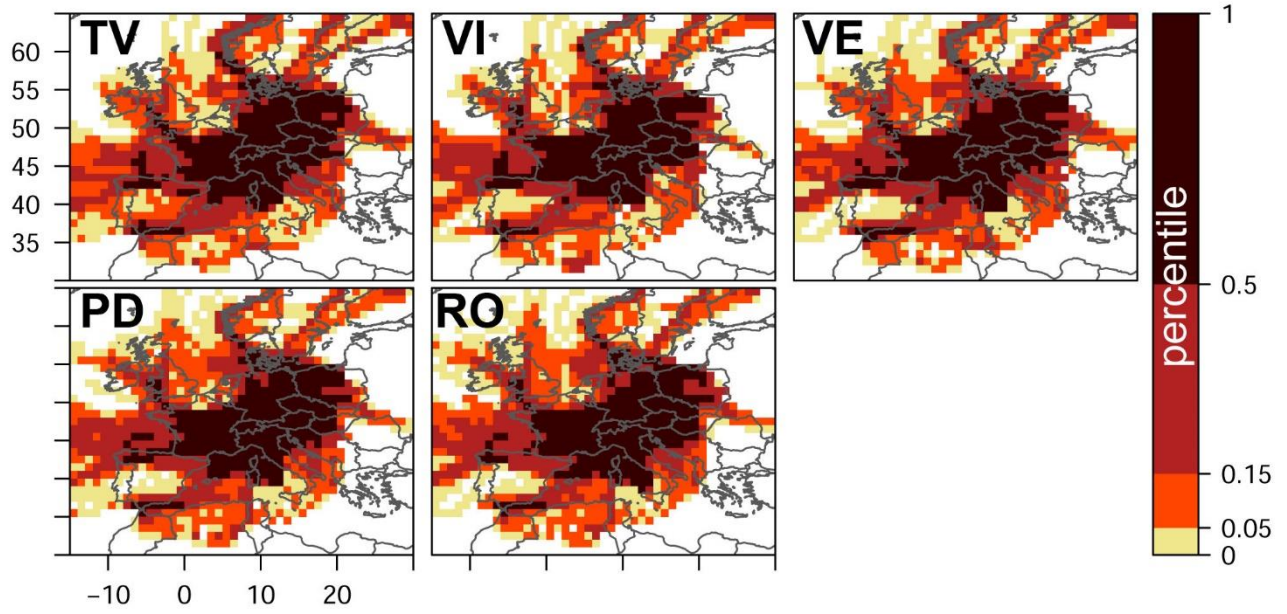

Figure S15. $N_{i,j}$ (percentile of the number of endpoints) used for the weighting functions. Details in Section S2.

References

Andrews, E., Saxena, P., Musarra, S., Hildemann, L.M., Koutrakis, P., McMurry, P.H., Olmez, I. and White, W.H., 2000. Concentration and composition of atmospheric aerosols from the 1995 SEAVS experiment and a review of the closure between chemical and gravimetric measurements. Journal of the Air & Waste Management Association, 50(5), pp.648-664.

ARPAV (Agenzia Regionale per la Prevenzione e Protezione Ambientale del Veneto), 2019. Emission Inventories (INEMAR) 2013 for the Municipalities in Veneto. [in Italian] available at: http://www.arpa.veneto.it/temi-ambientali/aria/file-e-allegati/dati-inemar-2013-def (last access March 2019).

Bencs, L., Ravindra, K., de Hoog, J., Rasoazanany, E.O., Deutsch, F., Bleux, N., Berghmans, P., Roekens, E., Krata, A. and Van Grieken, R., 2008. Mass and ionic composition of atmospheric fine particles over Belgium and their relation with gaseous air pollutants. Journal of Environmental Monitoring, 10(10), 1148-1157.

Chow, J.C., Watson, J.G., Fujita, E.M., Lu, Z., Lawson, D.R. and Ashbaugh, L.L., 1994. Temporal and spatial variations of PM2. 5 and PM10 aerosol in the Southern California air quality study. Atmospheric Environment, 28(12), pp.2061-2080.

EEA (European Environmental Agency), 2019. CORINE Land Cover / CLC 2012 website. https://land.copernicus.eu/pan-european/corine-land-cover/clc-2012 (last access March 2019)

Engelhart, G.J., Hildebrandt, L., Kostenidou, E., Mihalopoulos, N., Donahue, N.M. and Pandis, S.N., 2011. Water content of aged aerosol. Atmospheric Chemistry and Physics, 11(3), 911-920.

ISTAT, 2019. 2011 Population and housing census. Available at: http://dati-censimentopopolazione.istat.it/Index.aspx?lang=en (last access March 2019)

Maenhaut, W., Schwarz, J., Cafmeyer, J. and Chi, X., 2002. Aerosol chemical mass closure during the EUROTRAC-2 AEROSOL Intercomparison 2000. Nuclear Instruments and Methods in Physics Research Section B: Beam Interactions with Materials and Atoms, 189(1-4), pp.233-237.

Marcazzan, G.M., Vaccaro, S., Valli, G., Vecchi, R., 2001. Characterisation of PM10 and PM2.5 particulate matter in the ambient air of Milan (Italy). Atmos. Environ. 35, 4639–4650.

Masiol, M., Squizzato, S., Ceccato, D., Rampazzo, G. and Pavoni, B., 2012. Determining the influence of different atmospheric circulation patterns on PM10 chemical composition in a source apportionment study. Atmospheric Environment, 63, pp.117-124.

Masiol, M., Formenton, G., Pasqualetto, A. and Pavoni, B., 2013. Seasonal trends and spatial variations of PM10-bounded polycyclic aromatic hydrocarbons in Veneto Region, Northeast Italy. Atmospheric Environment, 79, 811-821.

Masiol, M., Formenton, G., Giraldo, G., Pasqualetto, A., Tieppo, P. and Pavoni, B., 2014a. The dark side of the tradition: The polluting effect of Epiphany folk fires in the eastern Po Valley (Italy). Science of the Total Environment, 473, 549-564.

Masiol, M., Squizzato, S., Rampazzo, G. and Pavoni, B., 2014b. Source apportionment of PM2. 5 at multiple sites in Venice (Italy): spatial variability and the role of weather. Atmospheric Environment, 98, 78-88.

Masiol, M., Agostinelli, C., Formenton, G., Tarabotti, E. and Pavoni, B., 2014c. Thirteen years of air pollution hourly monitoring in a large city: potential sources, trends, cycles and effects of car-free days. Science of the Total Environment, 494, 84-96.

Masiol, M., Squizzato, S., Formenton, G., Harrison, R.M. and Agostinelli, C., 2017. Air quality across a European hotspot: Spatial gradients, seasonality, diurnal cycles and trends in the Veneto region, NE Italy. Science of The Total Environment, 576, 210-224.

Masiol, M., Squizzato, S., Rich, D.Q., Hopke, P.K., 2019. Long-term trends (2005–2016) of source apportioned PM2.5 across New York State. Atmospheric Environment, 201, 110-120.

Perrone, M.G., Larsen, B.R., Ferrero, L., Sangiorgi, G., De Gennaro, G., Udisti, R., Zangrando, R., Gambaro, A. and Bolzacchini, E., 2012. Sources of high PM2. 5 concentrations in Milan, Northern Italy: molecular marker data and CMB modelling. Science of the Total Environment, 414, pp.343-355.

Rampazzo, G., Masiol, M., Visin, F. and Pavoni, B., 2008. Gaseous and PM 10-bound pollutants monitored in three sites with differing environmental conditions in the Venice area (Italy). Water, Air, and Soil Pollution, 195(1-4), 61-176.

Squizzato, S., Masiol, M., Visin, F., Canal, A., Rampazzo, G. and Pavoni, B., 2014. The PM 2.5 chemical composition in an industrial zone included in a large urban settlement: main sources and local background. Environmental Science: Processes & Impacts, 16(8), 1913-1922.

Squizzato, S., Masiol, M., Agostini, C., Visin, F., Formenton, G., Harrison, R.M. and Rampazzo, G., 2016. Factors, origin and sources affecting PM1 concentrations and composition at an urban background site. Atmospheric Research, 180, 262-273.

Squizzato, S., Cazzaro, M., Innocente, E., Visin, F., Hopke, P.K. and Rampazzo, G., 2017. Urban air quality in a mid-size city—PM2. 5 composition, sources and identification of impact areas: From local to long range contributions. Atmospheric Research, 186, pp.51-62.